Mixed cation effect in chalcogenide glasses Rb_2S-Ag_2S-GeS_2

C. Rau,[1,*] P. Armand,[1] A. Pradel,[1,†] C. P. E. Varsamis,[2] E. I. Kamitsos,[2] D. Granier,[1] A. Ibanez,[3] and E. Philippot[1]
[1]*Laboratoire de Physicochimie de la Matière Condensée, UMR 5617 CNRS, Université Montpellier II, CC 003, 34095 Montpellier Cedex 5, France*
[2]*Theoretical and Physical Chemistry Institute, NHRF, 48 Vassileos Constantinou Avenue, 11635 Athens, Greece*
[3]*Laboratoire de Cristallographie, CNRS, F-38042 Grenoble Cedex 09, France*
(Received 6 November 2000; published 24 April 2001)

Chalcogenide glasses with composition $0.5[(1-x)Rb_2S$-$xAg_2S]$-$0.5GeS_2$, $0 \leqslant x \leqslant 1$, were prepared and their ion transport properties and glass transition temperatures were found to show clear manifestations of the mixed cation effect. These Rb-Ag thiogermanate glasses were shown to be homogeneous in the mesoscopic domain by small-angle x-ray scattering. Extended x-ray-absorption fine structure indicated that each mobile cation forms its own specific environment that is not influenced by the presence of the dissimilar cation. On the other hand, Raman and infrared spectra showed nonlinear structural changes of the glassy matrix upon cation mixing. The maximum deviation from structural additivity was observed for compositions giving the extreme values for conductivity and T_g, and was found to result from cation-triggered rearrangements of the local germanate polyhedra toward a more homogeneous glass structure. These results support the recently proposed CIRON model that focuses on cation-induced relaxations of the network in mixed cation glasses.

DOI: 10.1103/PhysRevB.63.184204 PACS number(s): 61.43.Fs, 61.10.Ht, 61.18.−j, 66.10.Ed

I. INTRODUCTION

Ionic conducting chalcogenide glasses have been studied extensively during the last 20 years because they exhibit conductivity larger by two to three orders of magnitude than that of their oxide counterparts, and this property makes them potential candidates as solid-state electrolytes.[1–5] While large effort has been directed toward investigations of structure and ion transport properties of single cation chalcogenide glasses,[6–16] to our knowledge, there are only two reports on the existence of a mixed cation effect in chalcogenide systems.[17,18] Such a phenomenon has been observed in many ion conducting glassy materials and manifests itself by a markedly nonlinear behavior of dynamic properties, such as ionic conductivity, electrical and mechanical relaxation, and glass transition temperature, when one type of cation is replaced by another at a fixed total cation content.[19–21]

While considerable theoretical effort has been made to explain the origin of the mixed cation effect no universally accepted theory has been proposed to date. Several microscopic models are based on specific spatial distribution of the metal cations, such as preferential pairing or clustering among unlike cations within alkali-rich clusters.[21–23] More recent models are based on experimental results on oxide glasses; these models state that each cation maintains its own environment even in the presence of a dissimilar cation,[24–26] and propose that the migration of metal ions of one type to sites previously occupied by metal ions of another type is strongly inhibited.[27,28] Studies of the structure of the glassy backbone, which provides sites for metal cations and pathways for their migration, and its dependence on cation mixing are limited and deal almost exclusively with oxide glasses.[29–35] A recent paper on mixed alkali-silicate glasses reports on a nonlinear structural evolution of the glass matrix with composition, in close relation with the nonlinear behavior of electrical properties.[36] This result led the authors to propose a model, i.e., the cation-induced relaxations of the network (CIRON), as providing insights into the mixed cation effect.

In this context, we report in this work the synthesis and study of a mixed cation chalcogenide family, i.e., glasses with composition $0.5[(1-x)Rb_2S$-$xAg_2S]$-$0.5GeS_2$, $0 \leqslant x \leqslant 1$. The purpose of this work is twofold; first, to confirm the presence of the mixed cation effect in chalcogenide glasses by measurements of electrical conductivity and glass transition temperature, and second, to investigate in details the glass structure aiming at getting information on the origin of the mixed cation effect in this glass system. Three different aspects of the glass structure were investigated: the homogeneity of glasses in the mesoscopic domain by small-angle x-ray scattering (SAXS), the environments of the mobile cations by Ag and Rb *K*-edge extended x-ray-absorption fine structure (EXAFS) experiments, and the structure of the glass backbone by Fourier-transform Raman and infrared spectroscopies.

II. EXPERIMENTAL PROCEDURES

Rb_2S starting material was prepared by solid-state reaction. Stoichiometric quantities of the pure elements, 99.99% Rb and 99.999% S, with total mass of ~3–5 g were placed in a silica reaction vessel under argon atmosphere. The vessel was heated in an electric furnace up to 300 °C with a heating rate of 0.1 °C/min and held at this temperature for 48 h. After slow cooling, crystallized Rb_2S (Ref. 37) was obtained as a white powder and stored under inert atmosphere in a glove box.

The low-temperature form β-Ag_2S (Ref. 38) was obtained from $AgNO_3$ and $Na_2S \cdot 9H_2O$. First, silver nitrate was dissolved in distilled water under magnetic agitation, and then $Na_2S \cdot 9H_2O$ was added slowly to the solution. The precipitated black powder, β-Ag_2S, was washed several times with distilled water and ethyl alcohol and dried under primary vacuum for a period of 24 h. Both c-Rb_2S and β-Ag_2S

were checked by x-ray diffraction and the results agree with the existing data in the literature.[37,38]

The preparation of the starting GeS_2 material was described elsewhere.[39] Bulk $0.5[(1-x)Rb_2S\text{-}xAg_2S]\text{-}0.5GeS_2$ glasses with composition $x=0$, 0.2, 0.4, 0.6, 0.8, and 1 were prepared from the starting materials in carbon-protected silica tubes, which were sealed under high vacuum. For a total solid-state reaction, the tubes were heated to 500 °C for 1 week. Finally, the melts were equilibrated for 2 h at 1000 °C before quenching into an ice-water bath. X-ray diffraction measurements were performed for checking the amorphous state of the prepared samples.

Glass transition temperatures T_g were measured by differential scanning calorimetry (Setaram DSC 121) with a scanning rate of 10 °C/min. Due to the high reactivity of sulfide glasses with oxygen at elevated temperatures, and the slightly hygroscopic nature of the samples, the data collection was carried out in evacuated silica ampoules.

Disklike samples with 10 mm diameter and 1 mm thickness were prepared for electrical measurements. Gold electrodes were sputtered on both sides of the disk. Conductivity measurements were carried out with a HP4192A impedance-analyzer in the frequency range 10 Hz to 13 MHz with temperatures in range 25–250 °C.

SAXS measurements were done in order to check the homogeneity of the glasses on a scale of 10–1000 Å. Glass sheets with an optimal thickness of 80 μm were obtained with the twin-roller quenching technique in an argon-filled glove box.[40] The glass sheets were placed between two Kapton tapes to protect them from air and mounted on a modified Seifert diffractometer with a graphite monochromator to use the $K\alpha$ radiation of the turning copper anode. The scattering caused by the Kapton tape was subtracted from the experimental data. Both SAXS theory and data treatment are given elsewhere.[14]

For EXAFS experiments the glasses were ground and sieved to obtain powders with a regular grain size of 20 μm. The mass of glass powder had been previously computed to avoid saturation effects and to optimize the signal-to-noise ratio. The glass powders were mixed with cellulose and pressed as disk pellets. Silver (25 514 eV) and rubidium (15 200 eV) *K* edges absorption spectra were measured in transmission mode at LURE (Orsay, France) on the D44 beamline of the DCI storage ring operating at 1.85 GeV with an average current of 250 mA. All experiments were done at 35 K using a liquid-helium cryostat. The energy selection was made using a Si(311) double-crystal monochromator. Considering the high energy of the *K* edges studied, no rejection harmonic mirrors were used.

The EXAFS data were treated as described in detail elsewhere.[41] For the data analysis, the program package of Michalowicz was used.[42] The different steps of the experimental data exploitation were the same at the silver and rubidium edges and are briefly described here. For each of the samples studied (glasses and references) the zero-point energy E_0 is taken at the inflection point. The normalized Ag (Rb) *K*-edge EXAFS oscillations were k^3 weighted and Fourier transformed to the real space through a Kaiser window with $\tau=3$ (3.5) between 3.6 (3.3) and 12 (11.8) $Å^{-1}$. Then, the signal corresponding to the first coordination shell around Ag (Rb) atoms was isolated using a back Fourier transform. The simulations of the Fourier-filtered experimental signals have been performed with mean-square fitting procedure using experimental phase and amplitude functions from crystalline reference samples. This approach leads to the determination of the structural parameters, i.e., coordination number *N*, bond length *R*, and the Debye-Waller factor, $\Delta\sigma \approx \sigma_{\text{glass}} - \sigma_{\text{ref}}$.

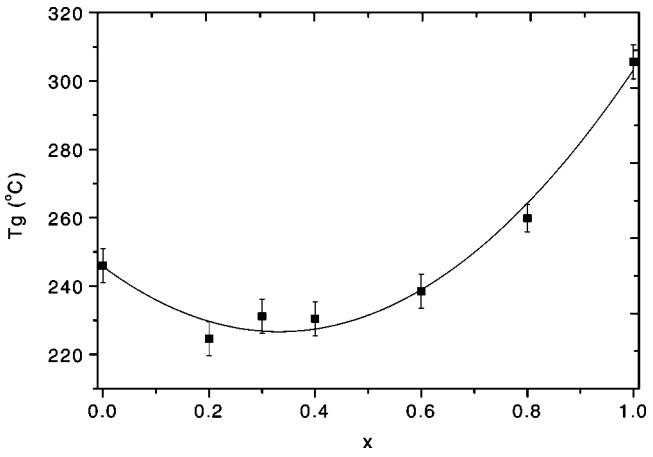

FIG. 1. Glass transition temperatures T_g for $0.5[(1-x)Rb_2S\text{-}xAg_2]\text{-}0.5GeS_2$ glasses. Lines are drawn to guide the eye.

Infrared specular reflectance spectra were recorded at quasinormal incidence (11°) on a Fourier-transform vacuum spectrometer (Bruker IFS 113V). All measurements were performed at room temperature in the spectral range 30–5000 cm^{-1} with a resolution of 2 cm^{-1}. The reflectance spectra were subsequently analyzed by the Kramers-Kronig (K-K) transformation to yield the optical response functions of the glasses.

Raman spectra were measured on a Fourier-transformed Raman instrument (Bruker RFS100) with a back-scattering geometry and a resolution of 2 cm^{-1}. The 1064.4-nm line of a Nd-Y laser was used for excitation and this led to a Raman spectra free of luminescence background. In our previous study on silver thiogermanate glasses, the Raman spectra measured with 514.5-nm excitation were found to exhibit fluorescence background especially at high Ag_2S contents.[9]

III. RESULTS

Glass formation in the system $0.5[(1-x)Rb_2S\text{-}xAg_2S]\text{-}0.5GeS_2$ was obtained over the whole range of compositions, $0 \leqslant x \leqslant 1$. Glass transition temperature $T_g(x)$ is shown in Fig. 1 and exhibits a negative deviation from additivity, with its minimum observed for compositions in the range $0.2 \leqslant x \leqslant 0.4$. The room temperature conductivity $\sigma_{20\,°C}$ and the activation energy E_a, derived from the Arrhenius dependence of conductivity with temperature, $\sigma = \sigma_0 \exp(-E_a/kT)$, are plotted as a function of x in Fig. 2. It is found that the nonlinear behavior of the ion transport properties is closely related to that of T_g. The minimum of both T_g and $\sigma_{20°\,C}$ is observed in the same composition range,

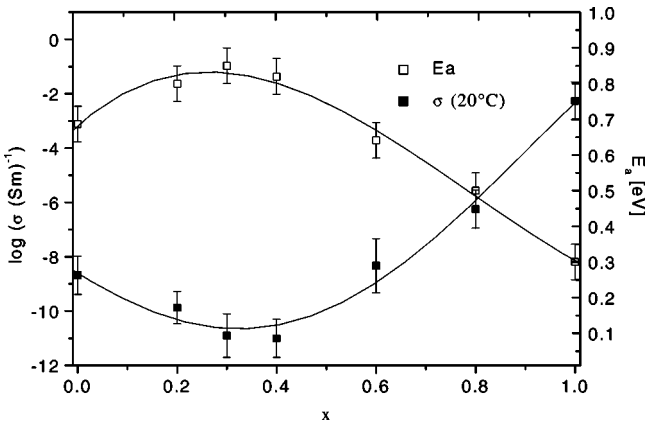

FIG. 2. Conductivity at 20 °C, σ_{dc}, and activation energy, E_a, as a function of composition for $0.5[(1-x)Rb_2S$-$xAg_2S]$-$0.5GeS_2$ glasses. Lines are drawn to guide the eye.

$0.2 \leqslant x \leqslant 0.4$, whereas E_a exhibits its maximum value in this range (Figs. 1 and 2).

In order to check whether the nonlinear evolution exhibited by the electrical properties and T_g is due to phase separation, as shown recently for glasses based on mixed glass-formers,[14] a SAXS investigation was undertaken. The results showed no significant scattering at small angles, and thus each glass can be considered as being homogeneous in the mesoscopic scale.

Due to the high energy of silver *K* edge (large core-hole width), rather weak ratios of signal to noise were obtained for the normalized EXAFS oscillations (Fig. 3). The *k* range restriction at $k_{max}=12\,Å^{-1}$, due to an important increase of the noise at higher energies, induces truncation effects by Fourier transforming. This is illustrated in Fig. 4 where the Fourier transformed (FT) modulus of $0.5[0.8Rb_2S$-$0.2Ag_2S]$-$0.5GeS_2$ glass is presented without correction for phase shift. In all cases, only the first silver coordination shell has been revealed. Fourier-filtered experimental signals are shown in Fig. 5 and present a very similar shape, characteristic of a back-scattering process of light atoms, e.g., sulfur. This suggests that the silver environment in these glasses should be rather similar.

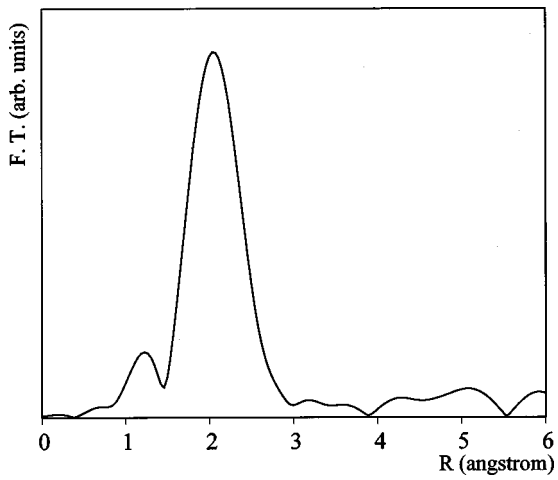

FIG. 4. Ag *K*-edge FT modulus (uncorrected for phase shift) of $0.5[0.8Rb_2S$-$0.2Ag_2S]$-$0.5GeS_2$ glass.

The Fourier-filtered oscillations of glasses have been well simulated by fitting simultaneously the structural parameters *N*, *R*, $\Delta\sigma$, and ΔE_0 in a one-shell model (silver surrounded only by sulfur atoms). Experimental backscattered phases and amplitudes were calculated from the 35 K EXAFS spectrum of CdS recorded at the Cd *K* edge (26 711 eV), as already done in a previous work on binary Ag_2S-GeS_2 glasses.[8] The wurtzite-type structure of CdS (Ref. 43) is characterized by regular CdS tetrahedra with bond lengths of 2.52 Å. The quantitative results for the mixed cation glasses are given in Table I, and show that each silver atom is surrounded by 2.8 sulfur atoms at an average distance of 2.5 ± 0.01 Å. The rather high values obtained for the Debye-Waller factor ($\Delta\sigma \sim 0.08$ Å) show the distorted surroundings of silver atoms in these glasses.

Figure 6 illustrates the Rb *K*-edge-normalized EXAFS oscillations of $0.5[(1-x)Rb_2S$-$xAg_2S]$-$0.5GeS_2$ glasses with $x=0$, 0.2, 0.4, and 0.6. The corresponding FT magnitudes present a unique peak characterizing the rubidium local environment. Figure 7 compares the filtered Fourier oscillations for different compositions. The high similarity of these curves shows that the rubidium first coordination sphere is

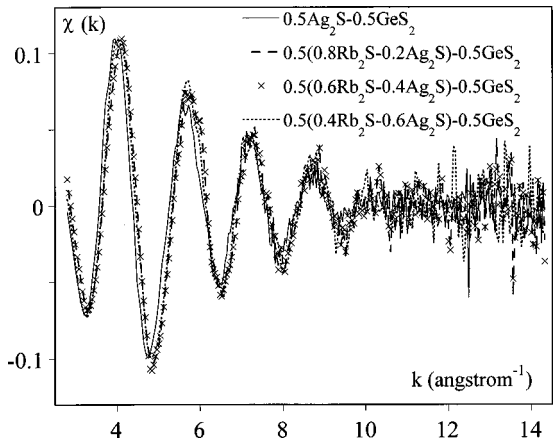

FIG. 3. Ag *K*-edge normalized EXAFS oscillations of $0.5[(1-x)Rb_2S$-$xAg_2S]$-$0.5GeS_2$ glasses.

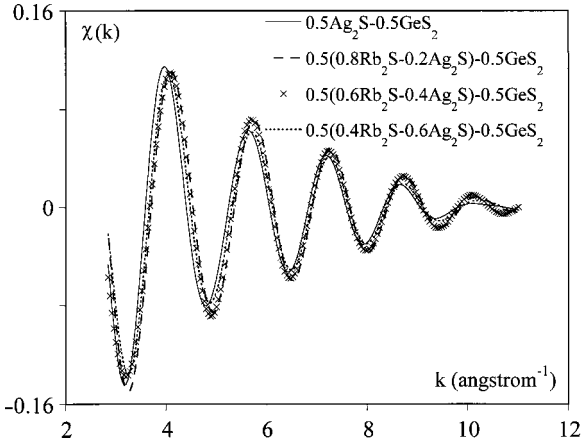

FIG. 5. Ag *K*-edge Fourier filtered oscillations of $0.5[(1-x)Rb_2S$-$xAg_2S]$-$0.5GeS_2$ glasses.

TABLE I. Ag *K*-edge fit results obtained for $0.5[(1-x)Rb_2S\text{-}xAg_2S]\text{-}0.5GeS_2$ glasses.

x	0.2	0.4	0.6	1
$N_{Ag\text{-}S}$	2.7±0.2	2.8±0.1	2.8±0.2	2.8±0.1
$\Delta\sigma$ (Å)	0.07±0.01	0.07±0.01	0.08±0.01	0.08±0.01
R (Å)	2.50±0.01	2.51±0.01	2.50±0.01	2.51±0.01
ΔE_0 (eV)	1.1±0.2	1.4±0.2	0.9±0.2	0.9±0.1

similar for all glasses. The simulations were made by using experimental backscattered phases and amplitudes extracted from the c-Rb_2S reference spectrum. In this crystalline phase, rubidium atoms are in regular tetrahedral sites with a Rb-S distance of 3.37 Å.[37] The fitted structural parameters are presented in Table II. For the whole glass compositions studied the average number of S surrounding Rb is 4.2 with an average distance of 3.38±0.01 Å. The distortion of sites hosting Rb ions is very high since $\Delta\sigma\sim0.14$ Å.

The FT-Raman spectra of the glasses investigated are shown in Fig. 8 for frequencies above 100 cm^{-1} where reliable Raman scattering is measured. All spectra present a well-defined and intense peak at ~330 cm^{-1} and additional peaks at ~370 and 410 cm^{-1}, with their relative intensity dependent strongly on glass composition. Besides these features, a weak shoulder is observed in the range 430–450 cm^{-1}.

The infrared absorption coefficient spectra, α (cm^{-1}), were obtained through K-K analysis and are reported in Fig. 9. A complex absorption envelope in the range 300–450 cm^{-1} dominates each infrared spectrum, and the profile of this envelope appears to be specific to each glass composition. In addition to this envelope, broad and weak bands are evident in the range 200–300 cm^{-1} and below 150 cm^{-1}.

As shown in Figs. 8 and 9 both Raman and infrared spectra of $0.5[(1-x)Rb_2S\text{-}xAg_2S]\text{-}0.5GeS_2$ glasses reveal changes in the relative intensity of bands, suggesting the occurrence of structural rearrangements upon gradual replacement of Rb_2S by Ag_2S.

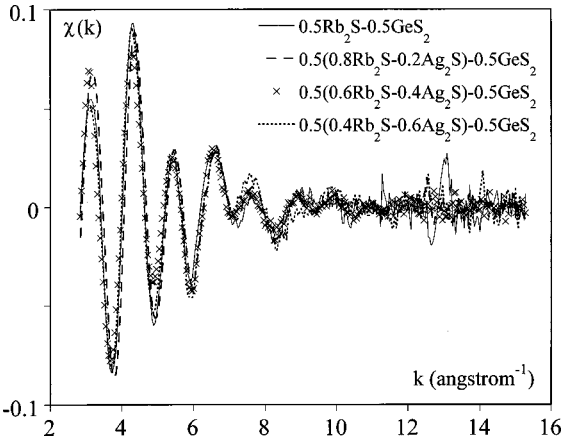

FIG. 6. Rb *K*-edge normalized EXAFS oscillations of $0.5[(1-x)Rb_2S\text{-}xAg_2S]\text{-}0.5GeS_2$ glasses.

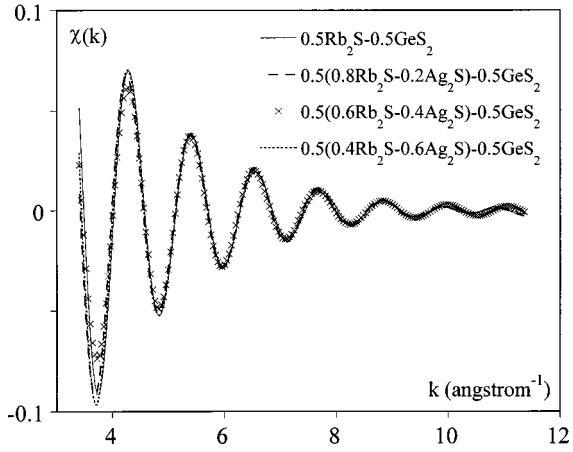

FIG. 7. Rb *K*-edge Fourier filtered oscillations of $0.5[(1-x)Rb_2S\text{-}xAg_2S]\text{-}0.5GeS_2$ glasses.

IV. DISCUSSION

A. Manifestations of the mixed cation effect in Rb-Ag thiogermanate glasses

The widely known mixed cation effect is usually associated with the nonlinear variation of conductivity when a glass modifier is progressively replaced by another, while keeping the total modifier content constant. As shown in Figs. 1 and 2 the ion transport properties as well as the glass transition temperature show clear manifestations of the mixed cation effect in the system $0.5[(1-x)Rb_2S\text{-}xAg_2S]\text{-}0.5GeS_2$. While mixed cation effects have been reported for many oxide glass systems[19–21] this is the second chalcogenide glass system found to exhibit the mixed cation effect.[17,18]

The fact that the composition range where T_g shows its minimum, $0.2\leqslant x\leqslant0.4$, coincides practically with the range of minimum in conductivity may indicate that some common structural characteristics may be related, through different dynamic mechanisms, to the manifestation of the mixed cation effect. In previous work on the mixed-glass-former effect in chalcogenide glasses $0.3Li_2S\text{-}0.7[(1-x)SiS_2\text{-}xGeS_2]$ (Ref. 14), SAXS results pointed out important structural changes with composition. In particular, it was shown that the mixed-glass-former effect could be attributed to the existence of phase separation in the range $0.50\leqslant x\leqslant0.64$. In this context, SAXS measurements were performed in this work on the $0.5[(1-x)Rb_2S\text{-}xAg_2S]\text{-}0.5GeS_2$ system in order to check the homogeneity of glasses. However, since no small-angle scattering was detected, all glass compositions

TABLE II. Rb *K*-edge fit results obtained with the reference c-Rb_2S for $0.5[(1-x)Rb_2S\text{-}xAg_2S]\text{-}0.5GeS_2$ glasses.

x	0	0.2	0.4	0.6
$N_{Rb\text{-}S}$	4.2±0.2	4.2±0.2	4.1±0.2	4.3±0.2
$\Delta\sigma$ (Å)	0.14±0.01	0.14±0.01	0.14±0.01	0.13±0.01
R (Å)	3.37±0.01	3.37±0.01	3.37±0.01	3.38±0.01
ΔE_0 (eV)	1.6±0.3	0.9±0.3	1.4±0.3	1.2±0.2

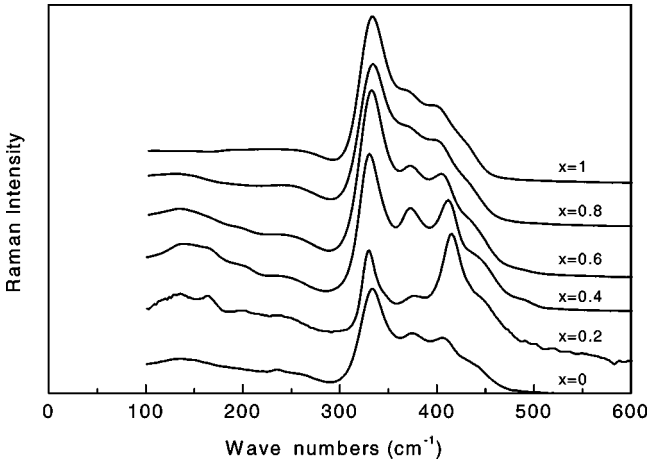

FIG. 8. FT-Raman spectra of $0.5[(1-x)Rb_2S$-$xAg_2S]$-$0.5GeS_2$ glasses.

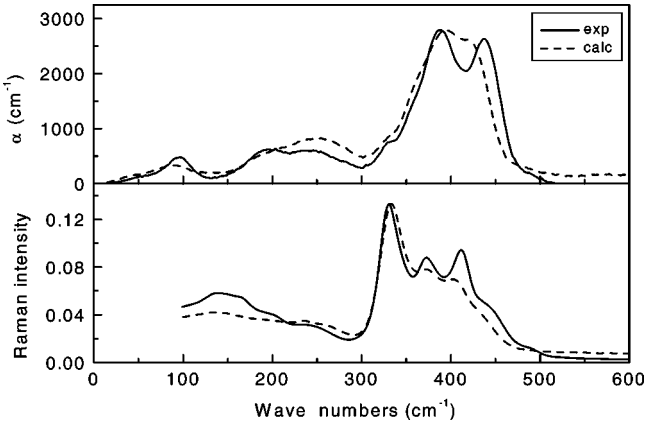

FIG. 10. Experimental Raman and infrared spectra of the $0.5[0.6Rb_2S$-$0.4Ag_2S]$-$0.5GeS_2$ glass compared with those calculated assuming linear combinations of the end-member spectra ($x=0$ and 1).

investigated here can be considered as homogeneous in the mesoscopic domain (10–1000 Å). This result indicates that structural models implying phase separation as the origin of the mixed cation effect[20,44] cannot be applied to this particular Rb-Ag thiogermanate system.

B. Cation environments in mixed Rb-Ag thiogermanate glasses

The parameters describing the local environment of Ag^+ and Rb^+ cations in $0.5[(1-x)Rb_2S$-$xAg_2S]$-$0.5GeS_2$ glasses were obtained from the analysis of the EXAFS data and are given in Tables I and II. Rubidium ions were found to be in tetrahedral sites formed by sulfur atoms, with an average Rb-S bond length of 3.38 Å similar to that encountered in crystalline Rb_2S. The high Debye-Waller factors found in this work ($\Delta\sigma \sim 0.14$ Å) support the existence of distorted RbS_4 sites. Silver ions occupy in these glasses also distorted sites, with an average of 2.8 sulfur atoms as first neighbors at a distance of ~2.51 Å. This bond distance being nearly the sum of covalent radii, combined with the low coordination number of silver suggest that the Ag-S bonding in these glasses presents a partial covalent character, as already suggested for similar glasses by other authors.[7,45] It is noted that the structural values obtained are averaged parameters and thus a coordination number of 2.8 may indicate that most silver ions are threefold coordinated by S atoms and some of them are in twofold sites.[12] The flexibility of silver ions to coordinate with oxygen and to occupy a range of different sites, depending on the charge density provided by oxygen, was demonstrated in glassy and crystalline Ag-borate systems.[46]

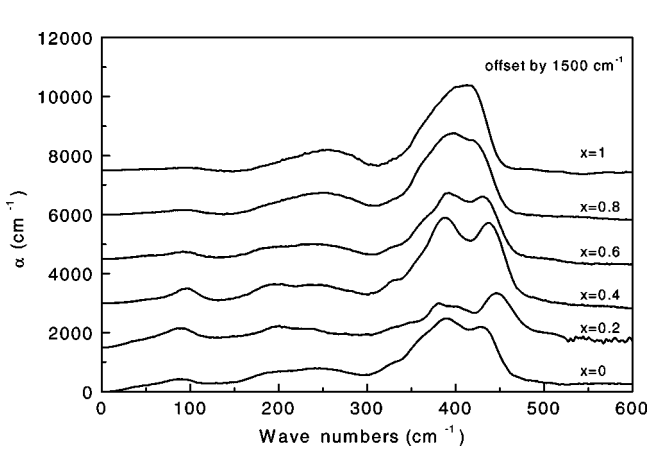

FIG. 9. Infrared absorption spectra of $0.5[(1-x)Rb_2S$-$xAg_2S]$-$0.5GeS_2$ glasses.

The results obtained at both silver and rubidium *K* edges show clearly that Rb^+ and Ag^+ ions form their own sites, which are specific to the bonding requirements of each metal ion. Within experimental error, no significant change in the first coordination environment of each metal ion was found to occur as a function of glass composition. Therefore, the first coordination shells around Rb^+ and Ag^+ ions are specific to each ion and the presence of an ion of second type does not seem to influence the local environment of the first ion, at least to a degree detectable by EXAFS. The present results are in good agreement with the original EXAFS findings of Greaves for mixed $0.5[K_2O$-$Cs_2O]$-$2SiO_2$ silicate glasses[24–26] and with more recent EXAFS results of Huang *et al.* for glasses in the system $0.2[(1-x)Rb_2O$-$xAg_2O]$-$0.8GeO_2$ (Ref. 47) and $0.2[(1-x)Rb_2O$-$xK_2O]$-$0.8GeO_2$ (Ref. 48). It is interesting to note that in the case of $0.2[(1-x)Rb_2O$-$xAg_2O]$-$0.8GeO_2$ glasses the first coordination shells of the two cations are quite different ($N_{Rb} \approx 6, N_{Ag} \approx 2$) compared to our results for the Rb-Ag thiogermanate glasses, but still the coordination shells were found to be independent of cation mixing.[47]

C. Effect of cation mixing on the thiogermanate glass network

As evidenced in Figs. 8 and 9 the Raman and infrared spectra of mixed $0.5[(1-x)Rb_2S$-$xAg_2S]$-$0.5GeS_2$ glasses change in a nonmonotonic way as x varies from one end-member ($x=0$) to the other ($x=1$). This effect is pronounced mainly for compositions $x=0.2$ and 0.4. To further

demonstrate this effect, we compare in Fig. 10 the experimental Raman and infrared spectra of the $x=0.4$ glass with the spectra calculated as linear combinations of the end-member spectra ($x=0$ and 1). It is noted that before calculation the end-member spectra were normalized with respect to the maximum value of the most intense peak, i.e., at ~335 and 380 cm^{-1} for the Raman and infrared spectra, respectively. The differences between the experimental and calculated spectra are obvious in Fig. 10, and thus show clearly that a simple linear mixing of the structures of the two end-member glasses cannot reproduce the thiogermanate structure of the cation-mixed glass. In order to understand the nature of the structural rearrangements triggered by cation mixing it is necessary to consider first the spectra of the single-alkali glasses.

The structure of GeS_2 glass can be described in terms of $GeS_{4/2}$ tetrahedra, (Q_4, according to silicate notation)[49,50] connected to each other by Ge-S-Ge bridges.[51–55] Addition of the modifier metal sulfide to GeS_2 leads to the creation of terminal Ge-S^- bonds through rupture of Ge-S-Ge bridging bonds.[54] Therefore, the Raman and infrared spectra of modified thiogermanate glasses can be discussed in terms of the vibrational characteristics of thiogermanate tetrahedral units Q_n containing 4-n terminal bonds, Ge-S^-, and n bridging bonds, Ge-S, per germanium atom. Barrau *et al.*[56] studied the Raman spectra of $y$$Na_2S$-(1−y)$GeS_2$ glasses in a broad composition range, and compared the spectra of glasses with those of crystalline Na-thiogermanate compounds at the dithiogermanate ($y=0.33$), metathiogermanate ($y=0.5$), and pyrothiogermanate ($y=0.60$) compositions. It was shown that the frequency of the symmetric stretching vibration of the Q_n tetrahedral unit, ν(Ge-S^-), is sensitive to the number of terminal Ge-S^- bonds per germanium center ($4-n$), i.e., it decreases upon increasing the degree of network depolymerization brought about by increasing the Na_2S content. In particular, it was found that ν(Ge-S^-) appears at ~480 cm^{-1} for dithiogermanate units ($GeS_{3/2}S^- = Q_3$),420 cm^{-1} for metathiogermanate units ($GeS_{2/2}S_2^{2-} = Q_2$), and 400 cm^{-1} for the pyrogermanate tetrahedra ($GeS_{1/2}S_3^{3-} = Q_1$). The second intense Raman band that involves mainly the stretching vibration of bridging bonds, ν(Ge-S), is less sensitive to Na_2S content of the glass and appears in the range 355–345 cm^{-1} for compositions between the dithiogermanate and pyrothiogermanate stoichiometries. Nevertheless, the intensity of the ν(Ge-S) band decreases progressively relative to that of ν(Ge-S^-) as the Na_2S content increases from the dithiogermanate ($y=0.33$) to the pyrothiogermanate ($y=0.60$) composition.[56] A very similar trend was observed recently in the Raman spectra of Rb-germanate glasses regarding the ν(Ge-O^-) frequency of Q_n germanium-oxygen tetrahedral units.[57]

By comparison to the above Raman results for the Na_2S-GeS_2 system, and arguments advanced earlier,[9] we attribute the high frequency features at 370–375 cm^{-1}, 400–405 cm^{-1}, and 425–440 cm^{-1} of the $x=0$ and $x=1$ Raman spectra to ν(Ge-S^-) of Q_1, Q_2, and Q_3 thiogermanate tetrahedral units, respectively. The cation-mass dependence of this frequency, i.e., its decrease from Na to Rb to Ag for each Q_n unit, is understood by the fact that the coordination sphere of metal cations consists mainly of terminal S atoms. To explain the coexistence of the different Q_n species at the metathiogermanate composition, where normally one would expect only the Q_2 arrangements, it was proposed[9] that the following equilibria take place in the melt and are partially quenched in the glassy state:

$$3Q_2 \rightleftarrows Q_4 + 2Q_1, \tag{1}$$

$$2Q_2 \rightleftarrows Q_3 + Q_1. \tag{2}$$

The formation of Q_4 species, besides Q_1 and Q_3, is consistent with the high relative intensity of the 333 cm^{-1} band because the symmetric stretching vibration of $GeS_{4/2}$ tetrahedra gives a strong Raman band at 340 cm^{-1}.[9]

We return now to the effect of Rb/Ag mixing on the Raman spectra and observe in Fig. 8 that the band at 415 cm^{-1} gains relative intensity in the composition range $0.2 \leqslant x \leqslant 0.4$ in comparison to the end-member spectra. While this band is in the range of υ(Ge-S^-) in Q_2 units, its higher frequency compared to the end-member frequencies may signify local strain effects. Such effects could result from localized deformations that the network has to undergo in order to accommodate the size mismatch of dissimilar cations in neighboring anionic sites. The clear increase of the relative intensity of the Q_2 band upon cation mixing can be interpreted now by a progressive shift of equilibria (1) and (2) to the left in cation mixed glasses. Therefore, cation mixing appears to result in a more homogeneous glass structure, since Q_2 units are formed at the expense of Q_4, Q_3, and Q_1 species, which, in the first place, are not expected by stoichiometry. This structural homogeneity may facilitate the creation of neighboring anionic sites hosting the dissimilar cations.

We examine now whether the structural picture developed by considering the Raman spectra is consistent with the composition dependence of the corresponding infrared spectra (Fig. 9). While the high-frequency profile (300–500 cm^{-1}) of the Raman spectra is dominated by the symmetric stretching modes of the Q_n species, the asymmetric stretching modes of the same species give strong absorption bands in the high-frequency range of the infrared spectra. For isolated tetrahedral species of point group T_d (such as the Q_4 and Q_0 tetrahedra) group theory predicts the following normal modes of vibration: $\Gamma_{T_4} = A_1(R) + E(R) + 2T_2(\mathrm{IR},R)$, with R and IR indicating Raman and infrared activity, respectively. The T_2 mode corresponds to the asymmetric stretching vibration that is particularly strong in the infrared. When the T_d point group symmetry is reduced to C_{3v}, as in the case of Q_3 and Q_1 tetrahedra, then the A_1 and E modes acquire infrared activity and the T_2 mode splits into two components: $T_2(\mathrm{IR},R) = A_1(R,\mathrm{IR}) + E(R,\mathrm{IR})$. Thus, instead of one band, the asymmetric stretching of Q_3 and Q_1 tetrahedra would give in the infrared two component bands. Further reduction of the T_d symmetry to C_{2v} would cause complete lifting of degeneracy of the T_2 mode, $T_2(\mathrm{IR},R) = A_1(R,\mathrm{IR}) + B_1(\mathrm{IR},R) + B_2(\mathrm{IR},R)$. It is noted that the met-

athiogermanate tetrahedral units (Q_2) have the C_{2v} point group symmetry, and thus the asymmetric stretching vibration of these units is expected to result in three components in the high-frequency part of the infrared spectrum.

The above considerations show the complexity of the infrared with respect to Raman, where the nondegenerate A_1 modes dominate the spectrum. Thus, it is clear that it is not possible to attribute each component band in the high-frequency region of the infrared to a specific Q_n unit, considering the coexistence of species with $n=4,3,2,1$. It is also evident that creation of Q_2 tetrahedra adds to the complexity of the infrared spectrum since these species give the largest possible number of components in the infrared. With this information in mind we note from Fig. 9 that the spectrum of the $x=0.2$ mixed cation composition gives a better resolution in the 300–500 cm^{-1} region than any other glass. This is compatible with the presence of the largest relative population of Q_2 tetrahedra in the $x=0.2$ glass, in good agreement with the results reached from the Raman spectra.

Therefore, we may conclude that both Raman and infrared spectra suggest that the presence of dissimilar cations leads to a more homogeneous glass structure, and this is effected by increasing the relative proportion of Q_2 units through shifting the melt equilibria involving Q_n species. If this is the case, then one may expect a more uniform distribution of anionic sites hosting the Rb^+ and Ag^+ cations, because these sites are formed by the sulfur atoms of the thiogermanate local units. While such a conclusion was not easy to deduce from the EXAFS analysis, the far-infrared region of the spectra may give useful trends. As shown in Fig. 9, the $x=0$ spectrum gives a weak band at ~ 90 cm^{-1} and the $x=1$ spectrum gives a corresponding feature at ~ 100 cm^{-1}. These bands can be attributed to the localized vibration of Rb^+ and Ag^+ ions, respectively, against their equilibrium sites as shown in previous studies.[9,32,46,58] It is observed in Fig. 9 that the Ag^+ motion band is significantly broader than that of Rb^+ ions. This result indicates the ability of Ag^+ cations to form a range of sites with different coordination numbers, in accordance with the Ag *K*-edge EXAFS analysis. For mixed cation glasses one band is observed at frequencies between 90 and 100 cm^{-1}, as a result of the overlapping contributions from the Rb^+ and Ag^+ cation-site vibration bands. What is of interest, though, is the sharpening of the cation motion band at ~ 95 cm^{-1} for $x=0.2$ and 0.4, suggesting a more homogeneous distribution of cation hosting sites, in agreement with the Raman and mid-infrared results.

It is noted that local structural rearrangements analogous to those found in this work were shown to operate in mixed alkali borate[32,33,59,60] and silicate glasses.[36] This phenomenon was termed cation-induced relaxations of the network structure (CIRON) and it was thought to be related to the various manifestations of the mixed alkali effect.[36] In single-cation glasses, the glass structure below T_g is considered to be fixed (''frozen'') and therefore cation motions are largely decoupled from structural relaxations occurring in the glass matrix.[61] What was proposed is that the same structural ''freezing-in'' process may not be completed at T_g in mixed cation glasses and, therefore, sub-T_g structural relaxations could be effective in mixed cation glasses.[36] Local network rearrangements between the Q_u germanate units were found in this work to be easily triggered by cation mixing, and such kind of rearrangements could be the origin of sub-T_g structural relaxations. According to the dynamic structure model of Ingram and co-workers[28,62] the mixed cation effect originates from the fact that dissimilar cations always create sites that are suitable to their size and bonding requirements. For a glass containing *A* and *B* cations A^+ will prefer to hop into vacant $\overline{A}$ sites and cations B^+ into $\overline{B}$ sites. When A^+ ions cannot avoid hopping into $\overline{B}$ sites additional mismatch energy is required for $\overline{B}$ to $\overline{A}$ site conversion. However, the required cation site conversions cannot be achieved without cooperative local-network rearrangements, such as those found in this work. In particular, it was demonstrated that in mixed Rb-Ag thiogermanate glasses the network adapts special ''mixed cation'' structures, by appropriate shifting of equilibria between local structures, in order to allow the guest cations to continue changing their cation neighbors even below T_g. The need for such ''mixed cation'' structures originates from the fact that the molar volume of the mixed Rb-Ag glass is less than that of the single Rb glass of the same cation content, and, thus, Rb cations in neighboring sites will inevitably be closer together in the mixed cation glass than would normally be the case. To minimize the resulting steric problems, the glass must have reordered itself to maximize its homogeneity, and to minimize the probability of the larger cations being forced to approach each other too closely.

V. CONCLUSIONS

Manifestations of the mixed cation effect were found in the synthesized chalcogenide glass family $0.5[(1-x)Rb_2S\text{-}xAg_2S]\text{-}0.5GeS_2$. The nonlinear evolution of the electrical parameters, σ_{dc} and E_a, was found to be followed by a similar behavior of T_g. Structural investigations by several techniques were carried out in order to understand the origin of this phenomenon. SAXS experiments showed that Rb-Ag thiogermanate glasses are homogeneous in the entire composition range, and EXAFS indicated that Rb^+ and Ag^+ cations form their own specific local environments, which are not affected by the presence of the dissimilar cation.

A nonlinear structural evolution of the glass matrix with composition (x) was pointed out by the study of the infrared and Raman spectra. The maximum structural deviation from additivity was found to correspond to the same composition range, $0.2 \leqslant x \leqslant 0.4$, where T_g and electrical parameters exhibit their extreme values. The detailed consideration of the vibrational spectra suggested that the presence of dissimilar cations in mixed glasses triggers a redistribution of local germanate polyhedra leading to a more homogeneous glass structure. It was discussed that this structural reorganization in mixed Rb-Ag glasses provides a mechanism to the network for relaxing steric effects related to larger Rb cations being forced in neighboring sites of the mixed glass. The same process leads the dissimilar cations to occupy neigh-

boring sites, which can be dynamically exchanged upon providing the required site mismatch energy. The present results provide support to the cation-induced relaxations of the network (CIRON) model,[36] which was proposed recently as being related to the origin of the mixed cation effect.

ACKNOWLEDGMENTS

Partial support of this work by the Greek-French bilateral R & D program (PLATON project) is gratefully acknowledged. The authors thank LURE for provision of the Synchrotron Radiation Facility.

*Present address: ESRF, BP220, F-38043 Grenoble Cedex, France.
†Corresponding author. FAX: 33 4 67 14 42 90. Email address: apradel@lpmc.univ-montp2.fr

[1] M. Ribes, B. Barrau, and J. L. Souquet, J. Non-Cryst. Solids **38–39**, 271 (1980).
[2] J. P. Malugani and G. Robert, Solid State Ionics **1**, 519 (1980).
[3] J. Kennedy and Y. Yang, J. Solid State Chem. **69**, 252 (1987).
[4] A. Pradel and M. Ribes, Mater. Chem. Phys. **23**, 121 (1989).
[5] A. Hayashi, M. Tatsumisago, and T. Minami, J. Electrochem. Soc. **146**, 3472 (1999).
[6] S. W. Martin, H. K. Patel, F. Borsa, and D. Torgeson, J. Non-Cryst. Solids **131–133**, 1041 (1991).
[7] R. J. Dejus, S. Susman, K. J. Volin, D. G. Montague, and D. L. Price, J. Non-Cryst. Solids **143**, 162 (1992).
[8] A. Ibanez, P. Armand, E. Philippot, and H. Dexpert, Solid State Ionics **59**, 157 (1993).
[9] E. I. Kamitsos, J. A. Kapoutsis, G. D. Chryssikos, G. Taillades, A. Pradel, and M. Ribes, J. Solid State Chem. **112**, 255 (1994).
[10] J. Kincs and S. W. Martin, Phys. Rev. Lett. **76**, 70 (1996).
[11] A. Pradel, G. Taillades, M. Ribes, and H. Eckert, J. Non-Cryst. Solids **188**, 75 (1995).
[12] J. H. Lee, A. P. Owens, A. Pradel, A. C. Hannon, M. Ribes, and S. R. Elliott, Phys. Rev. B **54**, 3895 (1996).
[13] E. Bychkov, V. Tsegelnik, Yu. Vlasov, A. Pradel, and M. Ribes, J. Non-Cryst. Solids **208**, 1 (1996).
[14] A. Pradel, C. Rau, D. Bittencourt, P. Armand, E. Philippot, and M. Ribes, Chem. Mater. **10**, 2162 (1998).
[15] A. Pradel, G. Taillades, C. Cramer, and M. Ribes, Solid State Ionics **105**, 139 (1998).
[16] M. Kawasaki, J. Kawamura, Y. Nakamura, and M. Aniya, Solid State Ionics **123**, 259 (1999).
[17] A. Pradel and M. Ribes, J. Non-Cryst. Solids **172–174**, 1315 (1994).
[18] B. Gee, H. Eckert, A. Pradel, G. Taillades, and M. Ribes, J. Non-Cryst. Solids **215**, 32 (1997).
[19] J. O. Isard, J. Non-Cryst. Solids **1**, 235 (1969).
[20] D. Day, J. Non-Cryst. Solids **21**, 343 (1976).
[21] M. D. Ingram, Phys. Chem. Glasses **28**, 215 (1987).
[22] C. T. Moynihan, N. S. Saad, D. C. Tran, and A. V. Lesikar, J. Am. Ceram. Soc. **63**, 458 (1980).
[23] R. K. Sato, R. J. Kirkpatrick, and R. K. Brow, J. Non-Cryst. Solids **143**, 257 (1992).
[24] G. N. Greaves, J. Non-Cryst. Solids **71**, 203 (1985).
[25] G. N. Greaves, Philos. Mag. B **60**, 793 (1989).
[26] G. N. Greaves, C. R. A. Catlow, B. Vessal, J. Charnock, C. M. B. Henderson, R. Zhu, S. Qiao, Y. Wang, S. J. Gurman, and S. Houde-Walter, in *New Materials and their Applications, 1990*, Proceedings of the 2nd International Symposium on New Materials and their Applications, edited by D. Holland, IOP Conf. Proc. No. 111 (Institute of Physics, London, 1990), p. 411.
[27] A. Bunde, M. D. Ingram, P. Maass, and K. L. Ngai, J. Non-Cryst. Solids **131–133**, 1109 (1991).
[28] A. Bunde, M. D. Ingram, and P. Maass, J. Non-Cryst. Solids **172–174**, 1222 (1994).
[29] K. Kamiya, S. Sakka, K. Matusita, and Y. Yoshinaga, J. Non-Cryst. Solids **38**, 147 (1980).
[30] W. Soppe, C. Van der Marel, and H. W. den Hartog, J. Non-Cryst. Solids **101**, 101 (1988).
[31] J. Zhong and P. J. Bray, J. Non-Cryst. Solids **111**, 67 (1989).
[32] E. I. Kamitsos, A. P. Patsis, G. D. Chryssikos, and J. A. Kapoutsis, in *Proceedings of the International Symposium on Glass Science and Technology, 1993*, edited by G. D. Chryssikos and E. I. Kamitsos, Vol. 23 of Chimica Chronica, New Series (Association of Greek Chemists, Athens, 1994), p. 245.
[33] E. I. Kamitsos, Y. D. Yiannopoulos, C. P. Varsamis, and H. Jain, J. Non-Cryst. Solids **222**, 59 (1997).
[34] J. Swenson, A. Matic, A. Brodin, L. Borjesson, and W. S. Howells, Phys. Rev. B **58**, 11 331 (1998).
[35] E. Ratai, M. Janssen, and H. Eckert, Solid State Ionics **105**, 25 (1998).
[36] M. D. Ingram, J. E. Davidson, A. Coats, E. I. Kamitsos, and J. A. Kapoutsis, Glass Sci. Technol. (Frankfurt/Main) **73**, 89 (2000).
[37] K. May, Z. Kristallogr. **94**, 412 (1936).
[38] R. Sadanaga and S. Sueno, Mineral. J. **5**, 124 (1967).
[39] E. Robinel, B. Carette, and M. Ribes, J. Non-Cryst. Solids **57**, 49 (1983).
[40] A. Pradel, T. Pagnier, and M. Ribes, Solid State Ionics **17**, 147 (1985).
[41] B. K. Teo and P. A. Lee, J. Am. Chem. Soc. **101**, 2815 (1979).
[42] A. Michailowicz, *EXAFS pour le Mac* (Société Française de Chimie, Paris, 1991), p. 102.
[43] F. Schossbenger, J. Electrochem. Soc. **102**, 22 (1955).
[44] J. Charles, J. Am. Ceram. Soc. **48**, 432 (1965).
[45] J. M. Oldale, J. Rennie, and S. R. Elliott, Thin Solid Films **164**, 467 (1988).
[46] C. P. Varsamis, E. I. Kamitsos, and G. D. Chryssikos, Phys. Rev. B **60**, 3885 (1999).
[47] W. C. Huang, H. Jain, and M. A. Marcus, J. Non-Cryst. Solids **180**, 40 (1994).
[48] W. C. Huang, H. Jain, and G. Meitzner, J. Non-Cryst. Solids **255**, 103 (1999).
[49] C. M. Schramm, B. H. Dejong, and V. Parziale, J. Am. Ceram. Soc. **106**, 4396 (1984).
[50] A. R. Grimmer, M. Magi, M. Hahnert, H. Stade, W. Wieker, and E. Lippmaa, Phys. Chem. Glasses **25**, 105 (1984).
[51] G. Lucovsky, F. L. Galeener, R. C. Keezer, R. H. Geils, and H. A. Six, Phys. Rev. B **10**, 5134 (1974).
[52] P. M. Bridenbaugh, G. P. Espinosa, J. E. Griffiths, J. C. Phillips, and J. P. Remeika, Phys. Rev. B **20**, 4140 (1979).
[53] P. Boolchand, J. Grothaus, M. Tenhover, M. A. Hazle, and R. K. Grasselli, Phys. Rev. B **33**, 5421 (1986).

[54] P. Armand, A. Ibanez, H. Dexpert, and E. Philippot, J. Non-Cryst. Solids **139**, 137 (1992).
[55] P. Armand, A. Ibanez, and E. Philippot, J. Solid State Chem. **104**, 308 (1993).
[56] B. Barrau, M. Ribes, M. Maurin, A. Kone, and J.-L. Souquet, J. Non-Cryst. Solids **37**, 1 (1980).
[57] E. I. Kamitsos, Y. D. Yiannopoulos, M. A. Karakassides, G. D. Chryssikos, and H. Jain, J. Phys. Chem. **110**, 11 755 (1996).
[58] E. I. Kamitsos, Y. D. Yiannopoulos, H. Jain, and W. C. Hung, Phys. Rev. B **54**, 9775 (1996).
[59] E. I. Kamitsos, A. P. Patsis, and G. D. Chryssikos, Phys. Chem. Glasses **32**, 219 (1991).
[60] C. P. E. Varsamis, E. I. Kamitsos, and G. D. Chryssikos, Phys. Chem. Glasses **41**, 242 (2000).
[61] C. A. Angell, Chem. Rev. **90**, 523 (1990).
[62] M. D. Ingram, Glass Sci. Technol. (Frankfurt/Main) **67**, 151 (1994).